

First results on a Cn2 profiler for GeMS

Angela Cortés¹, Benoit Neichel², Andrés Guesalaga¹, Francois Rigaut², Dani Guzman¹

¹ Pontificia Universidad Católica de Chile, 4860 Vicuña Mackenna, Casilla 7820436, Santiago, Chile.

² Gemini Observatory Southern Operations Center, Colina el Pino s/n, Casilla 603, La Serena, Chile.

Abstract. GeMS (the Gemini MCAO System) is a facility instrument for the Gemini-South telescope. The system includes five laser guide stars, three natural guide stars, three deformable mirrors optically conjugated at 0, 4.5 and 9km and one tip-tilt mirror. Some of its unique features include an embedded Cn2 SLODAR profiler which is described in this paper. The Cn2 profile is reconstructed from the slopes seen by the 5 high order WFS, each one pointing in a laser guide star direction. Residuals from the 16x16 subapertures WFSs and DM commands are used to obtain pseudo-open loop data for SLODAR, allowing us to reconstruct up to 16 layers. The paper describes the results obtained from different validation steps followed during the development of the technique, namely: numerical simulations, artificially generated turbulence via DMs excitation and the use of on-sky data obtained from different commissioning nights. We also present results from a wind profiler that runs in parallel to SLODAR and finally compare the results to those from a nearby MASS/DIMM instrument.

1. Introduction

The Cn2 is the refractive index structure parameter that quantifies the atmospheric optical turbulence. The knowledge of this vertical turbulence profile is particularly crucial to assist the tomographic process in a MCAO system [1]. Our goal is to estimate this profile in real time in order to optimize the tomographic reconstruction.

The first efforts to estimate this profile were introduced by Fusco [2] and Wilson [3]. Current techniques used to determine the Cn2 are mainly based on two approaches. One uses the correlation of the scintillation pattern produced by a binary star in a pupil plane, known as generalized SCIDAR (Scintillation Detection And Ranging). The other one uses the correlation of the wavefront slopes measured on a binary star, using a Shack-Hartmann wavefront sensor (SH-WFS). The latter technique known as SLODAR (SLOpe Detection And Ranging), is the basis for the work described in this paper. We use real time data from the current five SH-WFS to measure and correct the turbulence probed by five Laser Guide Stars (LGS) deployed in a “X” asterism on the sky.

2. Theoretical description of the method

Using the concept developed by Wilson [3-4] and Butterley [5], the SLODAR can be adapted to a system using LGS instead of NGS (Natural Guide Stars). This was already studied on the works done by Rigaut [1] and Gilles [6]. SLODAR method works as an optical triangulation for the measurement of the atmospheric optical turbulence profile Cn2, using the spatial covariance of the slopes (phase gradient of the wavefront phase aberrations received at the ground level), measured by WFSs, each pointing at a different LGS.

The turbulence profiling with LGS is performed to non-equispaced layer altitudes [6], due to the structure of the laser cone effect. The numbers of layers are determined by the number of the subapertures of the WFS, i.e. 16 layers here, and each altitude layer, when the telescope is pointing at zenith, is given by:

$$h = \frac{m \omega_0 z}{z \theta + m \omega_0} \quad (1)$$

where m is an integer ranging from 0 to 15, ω_0 is the size of the subaperture at the ground level, θ is the relative angular separation between the LGS pair (in GeMS, a square side of 60 arcseconds, see figure 1) and z is the altitude of the LGS. For this configuration and the LGS at 90km, we have two resolutions. For the high resolution (using just the ones in the square, not the one in the middle), the 16 altitudes are: 0, 1666, 3271, 4819, 6313, 7756, 9149, 10496, 11799, 13060, 14281, 15463, 16610, 17721, 18800, and 19846 m [7].

2.1. Modeling the turbulence

For the standard Kolmogorov model of the atmospheric turbulence, the spatial spectrum of aberrations at the ground is [8]:

$$\Phi(k) = 0.023 r_0^{-5/3} k^{-11/3} \quad (2)$$

Using this model, 16 turbulence layers were simulated and their corresponding slopes determined considering the structure of GeMS (five SH-WFS on an asterism configuration).

With the resulting slopes, the correlation matrix of all possible combinations of WFS are computed and averaged over time, so as to obtain estimations for the covariance among slopes. A data reduction technique that removes spatial redundancies was implemented, generating what is known as the covariance maps; this has shown to be very effective in reducing computational time [9].

The essence of the method is to fit the covariance maps obtained from WFS measurements to a weighted sum of the theoretical covariance maps and by retrieving the weighting factors, the turbulence profile is obtained [6].

Extensive simulations for different turbulence profiles were carried showing perfect agreement.

2.2. SLODAR in close-loop operation

Since the SLODAR technique assumes slopes from open-loop operation (full turbulence measurements), a reconstruction of the open loop from close-loop data is required. This is achieved by adding the residuals to the DMs voltages (V_{act}) projected onto the slope domain by

Adaptive Optics for Extremely Large Telescopes II

means of the interaction matrix (*iMat*) that corresponds to the static response of an AO system. This can be represented by the following equation:

$$Slopes_{POL}(k) = Slopes(k) + iMat * V_{act}(k - 1) \quad (4)$$

The interaction matrix corresponds to a matrix with a size of $N_{ms} \times N_{act}$, where N_{ms} is the number of measured slopes, and N_{act} is the number of actuators. It reflects the effect on the measured slope when a unit control signal is applied to the corresponding actuator, i.e. it characterizes the mapping between the DMs space and the WFSs space [9].

3. Calibration of the method with CANOPUS

CANOPUS, the AO bench of GeMS, consists of the opto-mechanical components of the Adaptive Optics Module (AOM) and the associated sensors, mechanism, and motors. It is mounted on a side looking port of the telescope Instrument Support Structure (ISS). A flat mirror folds the beam from the telescope, which is then collimated by an off-axis parabola onto three DMs conjugated at different elevations (0, 4.5 and 9 Km respectively) and a tip-tilt mirror (TTM). The three DMs are piezo stack type, leading to 917 actuators in total, but only 684 valid ones as seen by the WFSs and 233 extrapolated ones. The DM0 has 240 actuators active and 53 slaves with a pitch of 5mm, the DM4.5 has 324 actuators actives and 92 slaves with a pitch of 5 mm, and the DM9 has 120 active actuators and 88 slaves with a pitch of 10 mm [10].

A science beam splitter transmits the infrared light to the science path, and the 589 nm wavelength from the five laser beacons is reflected by the LGS beam splitter and sent to the LGS WFS. Each WFS is a Shack-Hartmann of 16x16 with 204 are valid subapertures, resulting to 2040 values of slopes (axis X and Y) and working at a sampling frequency of 800 Hz (maximum). The pixel size of the WFS is about 1.38'' and the measured read out noise of 3.5 *e*. Each subaperture on the CCD uses 2x2 pixels (quadcell) [11].

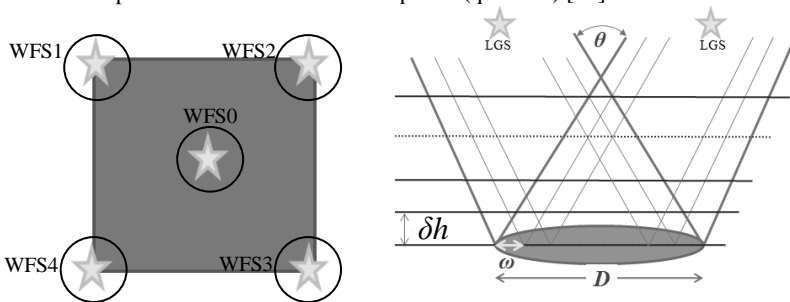


Fig. 1. Left: LGS asterism configuration; Right: SLODAR sampling layers

Using an internal calibration source to simulate the LGS and the 3 DMs to generate the turbulence at three altitudes, the method was tested in close-loop. By generating turbulence with the DMs at 0 km, 4.5 km and 9.0 km, we tested the fitting method, expecting a profile with concentrated energy at the corresponding altitudes. Good fittings were obtained for the first 2 altitudes, but at 9.0 km the estimation was spread onto neighboring layers, due to the

Adaptive Optics for Extremely Large Telescopes II

limited spatial resolution of DM9. This problem, however, is not relevant for the method since during on-sky operation the slopes are not frequency limited.

The second step that needed to be calibrated is the POL reconstruction of slopes. Data were taken from the bench in closed loop but with zero loop gain, applying a known turbulence on the DMs. Data in closed loop were also taken for the same turbulence and the scatter plots for two example subapertures for both sequences are shown in figure 2. A noticeable difference exists in the slope gain with respect to the ideal one and also a nonlinear effect due to the quad-cell dynamic range appears at higher values of slopes amplitudes. This showed to have low impact on the results and further normalization of slopes according to their r.m.s. (root mean square) values over time, proved to be very effective in reducing these possible sources of error.

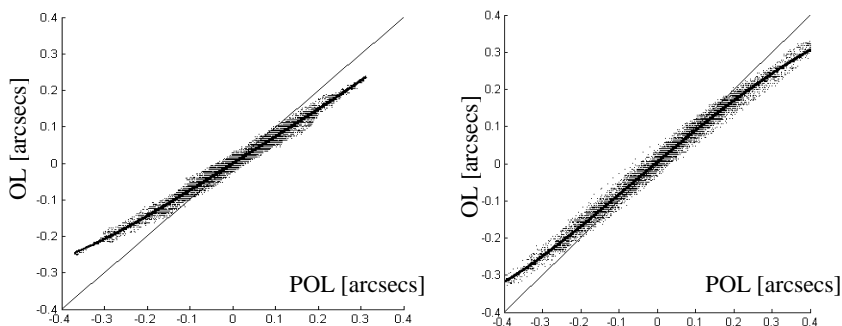


Fig. 2. Open Loop versus Pseudo Open Loop. The thin line is the ideal relationship that should be obtained; the thick line is a 4th order polynomial fit to the data (dot cloud). Left: WFS0 subaperture 1; Right: WFS1, subaperture 57

4. First on-sky results

Since lasers are launched from behind the secondary mirror, a contamination of the light received by the WFS occurs. This is the so-called fratricide effect [12, 13]. The number of affected subapertures can be determined by measuring the standard deviation of the slopes as clearly seen in figure 3 (left). Another source of strong distortions is caused by partially illuminated subapertures along the outer ring also shown in figure 3.

Adaptive Optics for Extremely Large Telescopes II

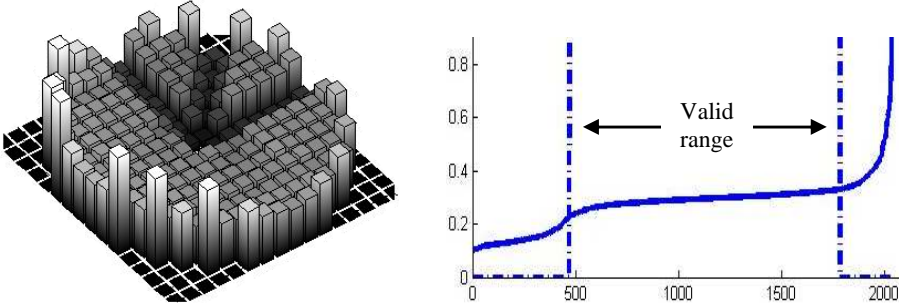


Fig. 3. Left: standard deviation of on-sky slopes, showing the fratricide effect and the partial illuminated subapertures. Right: slopes sorted according to their standard deviation. Values below the lower limit of the range correspond to the fratricide effect, and above to the partial illumination of the outer ring.

An automatic selection process based on the standard deviation of slopes was performed on the data in order to eliminate the distorted subapertures.

This method also eliminates some slopes that probably correspond to actuators that behave badly. It is important to filter first the bad data, to reduce the errors on the later fitting. This filter can be updated for every set of data or a common fixed one can be used for all the data. An example of typical mask is shown in figure 4.



Fig. 4. Remaining slopes after removing the subapertures with r.m.s. values outside the valid range.

After removing the noisy data, the fitting is performed on the measured covariance maps obtained on sky with the theoretical ones, to obtain the distribution of the turbulence in layers. Figure 5 show the results of the fitting for data from two different nights. The one on the left presents a non-typical profile for this site and a more typical profile is shown on the right.

In order to validate the SLODAR technique, two other approaches were also used, namely a wind profile [14], and data from a MASS-DIMM instrument located near the telescope.

The MASS-DIMM estimates the turbulence profile at 8 layers of the turbulence profile, but since MASS does not see the turbulence below 500 mts [15, 16], and its pointing may differ from that of GeMS, significant differences might occur.

We used MASS-DIMM data from the same night and time that for the SLODAR method and a cumulative plot of normalized sets of results are presented in figure 6. A good agreement between the two sets is obtained for the lower layers.

Adaptive Optics for Extremely Large Telescopes II

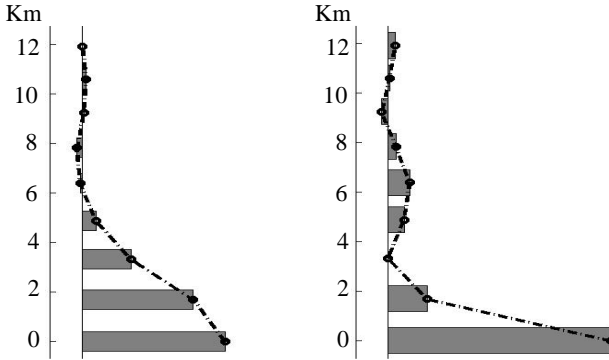


Fig. 5. SLODAR fitting for two different nights. Left: Apr 15th, 2011, at 23:55:15, Right: April 19th, 2011, from 06:16:24 to 06:21:25.

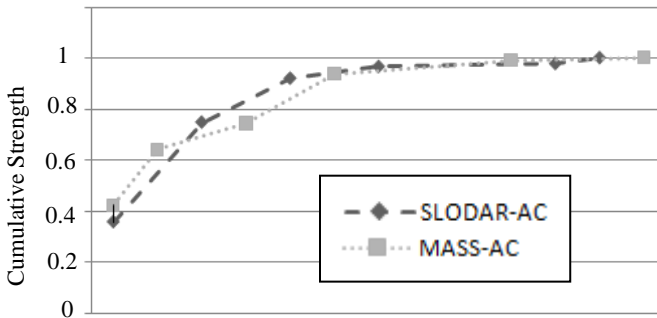


Fig. 6. Comparison between the profiles estimated using the SLODAR technique, and a MASS-DIMM close to the telescope, both from the same night (23:55, Apr 15th, 2011).

Then we compared the results using the wind profile technique, that is a similar concept to the covariance approach, but using the time-delayed cross-correlation between different wavefront sensors, as explained by Wang *et al* [14] and Gendron & Léna [17]. Wang uses NGS instead of LGS, thus cone and fratricide effects are not issues to consider. Gendron used time correlations from slopes generated by a single star, and they were able to determine the wind speed and direction.

The time cross-correlation is defined as:

$$C(\delta i, \delta j, \delta t) = \frac{\langle \sum_{ij} s_{ij}(t) s'_{i+\delta i, j+\delta j}(t + \delta t) \rangle}{O(\delta i, \delta j)} \quad (5)$$

where $s_{ij}(t)$ is the X or Y slope for subaperture (i, j) at time t , and $s'_{i+\delta i, j+\delta j}$ corresponds to a different wavefront sensor, moving on space and time. \sum_{ij} denotes the summation over all

overlapping illuminated subapertures, $\langle \rangle$ represent the averaging over the time series, and $O(\delta i, \delta j)$ is the number of overlapping illuminated subapertures for offset $(\delta i, \delta j)$. When $\delta t=0$, the method becomes the SLODAR technique, i.e. the pixel intensity along the baseline defined by the stars will correspond to different turbulent layers. Increasing the δt , will make the peaks of altitude turbulence move in opposite direction to the wind at each layer.

The results obtained with the wind profile supported the profile generated by the SLODAR technique, by allowing to check that estimated layers by SLODAR were also detected by the wind profiler at the previously estimated altitudes. We tested this method with the turbulence generated with the DMs and also with on-sky data.

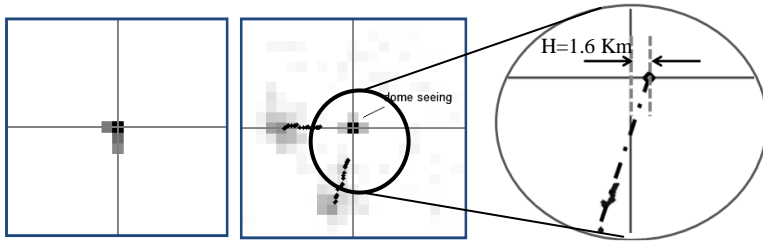


Fig. 7. The leftmost figures show the time correlation at $t=0$ and $t=0.4$ s, showing two layers moving in different directions and a third static peak at the center, corresponding to dome seeing. The right image shows how this technique can provide an altitude estimate by projecting the tracking path of turbulences onto the guide star baseline.

5. Conclusions

A SLODAR-based method to estimate turbulence profile (C_n^2) embedded in a MCAO system has been described. It uses the measured slopes from five LGS, and results have been satisfactorily compared to data from a wind profiler and a MASS-DIMM instrument. The C_n^2 profiler also proved to be useful to detect strong dome seeing. We are in the process of gathering more data, and automatize the procedure such as results will be available on-line for the optimization of the MCAO loop.

Acknowledgments

This work has been supported by the Chilean Research Council (CONICYT) through grant Fondecyt 1095153, Anillo ACT-86 and scholarship for first author. We are also grateful to Andrei Tokovinin, Tim Butterley and Tim Morris for fruitful discussions.

References

1. Rigaut, F. J., Ellerbroek, B. L., & Flicker, R. Principles, limitations, and performance of multiconjugate adaptive optics. Adaptive Optical Systems Technology, SPIE Proc., 4007, 1022-1031, (2000).

Adaptive Optics for Extremely Large Telescopes II

2. Fusco, T., Conan, J. M., Michau, V., Mugnier, L. M., & Rousset, G. Efficient phase estimation for large-field-of-view adaptive optics. *Optics letters*, 24(21), 1472-4, (1999).
3. Wilson, R. SLODAR: measuring optical turbulence altitude with a Shack–Hartmann wavefront sensor. *Monthly Notices of the Royal Astronomical Society*, 337(1), 103–108. Wiley Online Library, (2002).
4. Wilson, R. W., Butterley, T., & Sarazin, M. The Durham/ESO SLODAR optical turbulence profiler. *Monthly Notices of the Royal Astronomical Society*, 399(4), 2129–2138, (2009).
5. Butterley, T., Wilson, R. W., & Sarazin, M. (2006). Determination of the profile of atmospheric optical turbulence strength from SLODAR data. *Monthly Notices of the Royal Astronomical Society*, 369(2), 835-845.
6. Gilles, L., & Ellerbroek, B. Real-time turbulence profiling with a pair of laser guide star Shack–Hartmann wavefront sensors for wide-field adaptive optics systems on large to extremely large telescopes. *JOSA A*, 27(11), A76–A83. Optical Society of America, (2010).
7. Neichel, B., Rigaut, F., Bec, M., Boccas, M., Daruich, F., D’Orgeville, C., Fesquet, V., et al. The Gemini MCAO System GeMS: nearing the end of a lab-story. *Proceedings of SPIE (Vol. 7736, p. 773606)*, (2010).
8. Glindemann, A., Hippler, S., Berkefeld, T., & Hackenberg, W. Adaptive optics on large telescopes. *Experimental Astronomy*, 10(1), 5-47, (2000).
9. Quiros-Pacheco, F. *Reconstruction and Control Laws for Multi-conjugate Adaptive Optics in Astronomy*. Imperial College. (2006).
10. Neichel, B., Rigaut, F., Bec, M., & Garcia-Rissmann, A. Reconstruction Strategies for GeMS. 1st AO4ELT conference - Adaptive Optics for Extremely Large Telescopes, 02010, 02010. Les Ulis, France: EDP Sciences, (2010).
11. Rigaut, F., Neichel, B., Bec, M., Boccas, M., Garcia-Rissmann, A., & Gratadour, D. A Sample of GeMS Calibrations and Control Schemes. 1st AO4ELT conference - Adaptive Optics for Extremely Large Telescopes, 08001, 08001. Les Ulis, France: EDP Sciences, (2010).
12. Neichel, B., Rigaut, F. et al. “Sodium return, spot elongation and fratricide effect: first on-sky results with GeMS”, This conference (2011).
13. Wang, L., Otarola, A., & Ellerbroek, B. Impact of sodium laser guide star fratricide on multi-conjugate adaptive optics systems. *JOSA A*, 27(11), A19–A28. Optical Society of America, (2010).
14. Wang, L., Schöck, M., & Chanan, G. Atmospheric turbulence profiling with SLODAR using multiple adaptive optics wavefront sensors. *Applied optics*, 47(11), 1880-92. (2008).
15. Sarazin, M., & Roddier, F. The ESO differential image motion monitor, *A&A*, 227, 294. (1990).
16. V. Kornilov, A. A. Tokovinin, O. Vozyakova, A. Zaitsev, N. Shatsky, S. F. Potanin, and M. S. Sarazin. MASS: a monitor of the vertical turbulence distribution, *Adaptive Optical System Technologies II*. pp. 837-845 (2003).
17. Gendron, E., & Léna, P. Single layer atmospheric turbulence demonstrated by adaptive optics observations. *Astrophysics and Space Science*, 239(2), 221–228. Springer. (1996).